Hindawi
International Journal of Antennas and Propagation
Volume 2017, Article ID 6803019, 9 pages
https://doi.org/10.1155/2017/6803019

Research Article

Dual-Band RFID Antenna for 0.92 GHz Near-Field and 2.45 GHz Far-Field Applications

Zijian Xing, Kun Wei, Ling Wang, and Jianying Li

School of Electronics and Information, Northwestern Polytechnical University, Xi'an 710072, China

Correspondence should be addressed to Zijian Xing; xingzijian2004@126.com

Received 28 March 2017; Revised 26 April 2017; Accepted 1 June 2017; Published 10 July 2017

Academic Editor: Jaume Anguera

A novel antenna used in the near field of a 0.92 GHz and the far field of a 2.45 GHz RFID reader system is investigated. The new antenna achieves strong magnetic field distribution over 0.92 GHz with good performance of detecting tags when applied in FCC RFID systems, as well as a good performance of circular polarization at 2.45 GHz. Furthermore, the investigation shows the operation principle by circuit models and the advantages of the structure in terms of the operation frequency and field performances. The advantages of these two bands could be achieved by this novel RFID reader antenna.

1. Introduction

Radio frequency identification (RFID), which was developed around World War II, is a technology that provides wireless identification and tracking capability [1, 2]. Reader antennas are an important unit of RFID systems. Reader antennas can be classified into two classes by reading range for different application purposes: near-field (NF) antenna and far-field (FF) antenna. Operation frequencies of reader antennas include 125 KHz, 13.56 MHz, 433.92 MHz, UHF (ultrahigh frequency) 0.92 GHz, 2.45 GHz, and 5.8 GHz. Currently, 0.92 GHz and 2.45 GHz are more attractive because of their good performances of data speed and antienvironment jam ability [3–6].

Ultrahigh frequency (UHF) near-field RFID technology received a lot of attention due to its good performances in item-level RFID applications such as sensitive products tracking, pharmaceutical logistics, transport and medical products (blood, medicines, and vaccines), and biosensing applications [7–13]. The primary concern of UHF near-field RFID is to make the RFID system working in a short distance as reliable as that of the LF/HF near-field RFID. Inductive coupling systems are preferred in most applications of near-field UHF RFID, because most of the reactive energy is stored in the magnetic field. Magnetic coupling is stable in terms of the impact of liquid or metal. In contrast, capacitive coupling is the opposite because the energy is severely affected by high permittivity materials.

In the 2.45 GHz band, far-field circularly polarized RFID antennas receive more attention because of the high data speed and long identification distance. Because of these interrogation characters, energy transmission speed and efficiency are very important and have been studied a lot recently [14–18]. In far-field RFID systems, the RFID tags are always located in large range applications and the tags are normally single or dual linearly polarized (LP), and thus circularly polarized (CP) reader antennas are suitable for ensuring the stability of communications between readers and tags. Moreover, under most practical circumstances, other requirements for the reader antenna should be under consideration, such as structure sizes, acceptable gains, impedance bandwidths, multibands, and axial ratio (AR) bandwidths.

As advantages of these two standards, it is essential to integrate these two standards into one system. In this situation, a reader antenna covering 0.92 GHz near field and 2.45 GHz far field is a good design, which avoids using two single-band antennas. One challenge in RFID applications is to design such an antenna because the operation mode and frequency differences between 2.45 GHz far field and 0.92 GHz near field are too large to operate properly for dual-band structures [4–6]. Even though many dual-band RFID reader antennas are proposed, there are very few

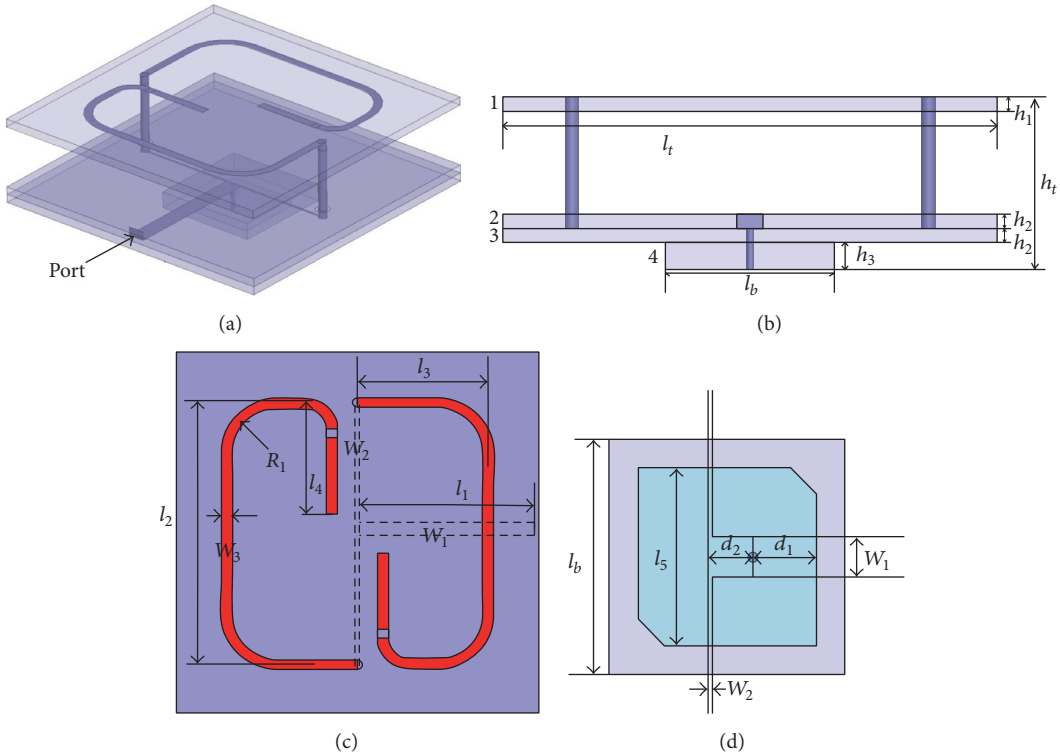

FIGURE 1: Model and structure of the proposed antenna: (a) 3D view, (b) side view, (c) top transparent view of the middle layer, and (d) bottom view of the circularly polarized antenna.

antennas that could fulfill this design goal. Most of the dual-band antennas are applied for far-field operation mode whereas most of the dual mode antennas are operated at the same frequency [19–21]. In [21], the dual-band 0.92/2.45 GHz unidirectional CP antenna is presented employing multiloops and a complex power splitter, but the operation modes of these two frequencies are all far field. In [22], the antenna can be operated in both near-field and far-field modes at a UHF band. However, these two operation modes share the same frequency, so that the total power is split into two components and then the efficiency of each mode will be decreased. There are also some papers that focus on the study of dual-band antennas [23, 24].

In this paper, a compact 0.92 GHz near-field and 2.45 GHz far-field dual-band antenna is proposed to generate strong magnetic field and circularly polarized wave, respectively. The two operation modes of the antenna are operated at different frequencies; the two modes work at different frequencies, so the efficiency of the two modes is high. But in [22], the two modes of operation work at the same frequency, so the energy is divided and the efficiency is reduced. The difficulty of this design is whether the feed network can establish high isolation between the two operation modes. Finally, the designing goal is achieved by the proposed antenna which is also investigated in detail. The methodology to complete impedance matching is addressed with the theory analysis. The structure, theory, and the performances of the antenna are analyzed in detail as follows.

This paper is organized as follows. Structure and modeling of the antenna will be introduced in Section 2. In Section 3, analysis and discussions are carried out to investigate the operation principle of the antenna and impedance matching theory. In Section 4, the performances of the antenna will be studied and analyzed. In the last part, conclusion will be given.

2. Modeling and Structure

The structure of the antenna is shown in Figure 1(a), which is composed of four layers which are FR4 layer 1, composite PTFE layer 2 and layer 3, and composite dielectric board layer 4. From the top layer to the bottom layer, these four layers are marked by numbers which are 1, 2, 3, and 4 in Figure 1(b). Layer 1 is mainly composed of two half-rectangle loops which have two folded straight terminals. Layer 2 and layer 3 are strip line feed network with lead printed onto the interface of the two, respectively. Fed at the edge of the bottom layer, 50-ohm strip transmission line is connected with one circularly polarized antenna and then split into two branches. The two branches are connected to two metal columns in another end. The other end of each column is connected to one metal half-rectangle loop strip. There is one load on each half-rectangle loop in Figure 1(a). Layer 1 and layer 2 are connected by two metal columns. A rectangle single feed circularly polarized antenna (layer 4) is fed by the main strip line and connected to

layer 3. The material of the circularly polarized antenna part is composite dielectric with low loss tangent.

Top layer 1 is the near-field antenna, and layer 2 and layer 3 are the feed network. Figure 1(b) shows the side view of the antenna. The circularly polarized antenna is located under layer 3. All of the sizes are marked in Figure 1(b), where height and square of the antenna is h_t and l_t, respectively. Thicknesses of FR4 PCB board and circularly polarized antenna are denoted by h_1, h_2, and h_3, respectively. The gap between layer 1 and layer 2 is h_g. In Figure 1(c), top view and transparent view of the feed network are shown, where all of the sizes are marked. The widths of 50-ohm transmission line and two branches are marked by W_1 and W_2, respectively. The sizes of the loop are marked by l_2, l_3, and l_4. Layer 4 is a circularly polarized antenna, and the edge lengths of the substrate and patch are marked by l_b and l_5, respectively.

3. Analysis and Discussion

The operation energies of the antenna include two parts which are 0.92 GHz near field and 2.45 GHz circularly polarized far field. In order to obtain good performances of the two modes, one challenge for designing the antenna is to establish high isolation between the near-field mode and the far-field mode, that is, less energy input to another mode at the operation frequency of one mode. The operation principle of the two modes and the theory analysis of the isolation technology are provided below.

The two half-rectangle loops of Figure 1(c) are a near-field antenna, which generate a strong magnetic field at 0.92 GHz. Two half loops are fed by one simple power splitter. The length of metal loops and the input impedance of the near-field antenna could be estimated based on resonant theory. If resonant frequency is determined, the total electric length of the metal column, half-rectangle loop, and folded terminal should match the resonant frequency. The rectangle half loop's mirror image function on the ground plane of the feed network needs to be considered. Metal columns should be long enough because the current mirror image is reversed and then will cancel out a part of the magnetic field. But if the metal column is too long, the current of the rectangle loop and magnetic field will be weak because the strong current section should be distributed on the columns. The effect of mirror image is discussed in [7]. Phase and magnitude of the current on both rectangle half loops are symmetrical so that the magnetic field can be strengthened simultaneously by the two branches of layer 1. Terminal stubs l_4 are useful for enhancing the current strength of the rectangle loops because the current of an open terminal is very weak. The rectangle circularly polarized antenna in layer 4 is a single feed antenna which operates at 2.45 GHz. The antenna is also fed by the same feed network which is composed of layer 2 and layer 3.

It is very important to design a feed network with appropriate feed points for these two operation modes, because the feed network structure brings about a huge influence on the efficiency of each radiation mode. The parallel circuit is composed of these two radiation parts which are near-field antenna and circularly polarized antenna. Figure 2 shows the equivalent circuit diagram which includes transmission lines and antennas. The resistance values and reactance properties are different at different frequencies.

In Figure 2, the equivalent circuits of two operation modes are marked. Input impedance of the circularly polarized antenna section and the near-field antenna section is replaced by $R_1 + X_1 * j$ and $R_2 + X_2 * j$, respectively. The input impedance of each antenna is not 50 ohms when the arbitrary frequency is different from its operation frequency. These two antenna sections form a parallel circuit and influence each other. The input impedance at each frequency is shown as

$$Z_{\text{in}} = \frac{(R_1R_2 - X_2X_1) + j(X_2R_1 + X_1R_2)}{R_1 + R_2 + j(X_2 + X_1)} = \frac{\left[R_1^2R_2 + R_1R_2^2 + X_2^2R_1 + X_1^2R_2 + j\left(X_2R_1^2 + X_1R_2^2 + X_2^2X_1 + X_2X_1^2\right)\right]}{(R_1 + R_2)^2 + (X_2 + X_1)^2}, \quad (1)$$

where Z_{in} is the port input impedance of the feed network in Figure 1(a). The antenna is composed of two parts. In (1), it is clear that the impedance of the feed point is influenced by these two antenna parts simultaneously at any frequency. In the general case, each part is fed by the input power at an arbitrary frequency. But it is a good design that most of the input energy is supplied to the part operating at its best resonant frequency, whereas less power is supplied to another part. In (1), resonance could be achieved when the imaginary part is equal to zero. Preferably, in case one part is operated at the resonant frequency, another part is operated at high impedance state because of the huge resonant frequency difference between these two parts. The operation states of these two parts have good performances by parameter optimization. The performances of antennas are analyzed in the next section in detail.

4. The Performances of the Antenna

The total height of this antenna is 25 mm, whereas the gap between layer 1 and layer 2 is h_g = 15 mm. A mirror effect of the near-field antenna exists on the ground plane of layer 2. If h_g is decreased, the mirror effect of the near-field antenna will be increased significantly, and vice versa. So h_g brings about a huge effect on the magnetic field strength of the near-field antenna. Actually, h_g = 15 mm is a very good choice in the design of near-field antennas. Other optimized parameters are shown as follows: h_t = 25 mm, l_t = 71.6 mm, h_1 = 2 mm, h_2 = 2 mm, h_3 = 4 mm, W_1 = 4.2 mm, W_2 = 0.5 mm, R_1 = 10 mm, l_1 = 30.55 mm, l_2 = 51.6 mm, l_3 = 25.8 mm, l_4 = 22 mm, l_b = 24.5 mm, l_5 = 18.5 mm, d_1 = 6.55 mm, and d_2 = 2.95 mm. In the condition of these parameters, two parts of the antenna can operate well at two frequencies.

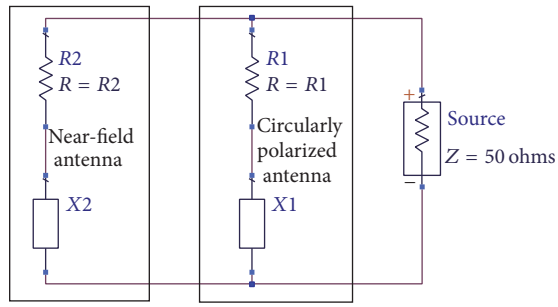

Figure 2: Equivalent feed network circuit of the two-antenna mode.

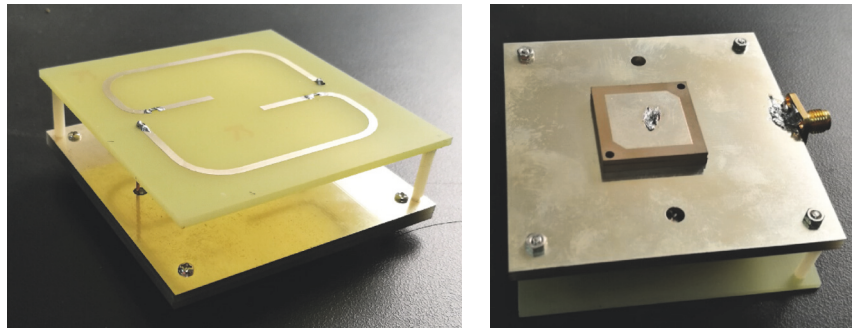

(a) (b)

Figure 3: Photo of the antenna: (a) front view and (b) back view.

A photo of the proposed antenna is shown in Figure 3. Figure 3(a) shows the front view of the antenna while Figure 3(b) shows the back view. Permittivity of the FR4, composite PTFE, and composite dielectric board is 4.4, 4.5, and 9.6, respectively. Loss tangent of the FR4, composite PTFE, and composite dielectric board is 0.02, 0.002, and 0.001, respectively. In the actual antenna structure, layer 1 and layer 2 are fixed by two nylon columns in order to make the antenna more stable. The permittivity of the columns is only 3.7 and far away from the conductors, so the columns almost bring about no effect on the performances of the antenna. The performances of the antenna are shown below.

4.1. S11 Performance. This novel antenna could be operated at two bands. S11 performances of the two bands are shown in Figure 4. The −10 dB bandwidth is also marked in Figure 4. In Figure 4, the comparison between measurement results and simulated ones shows that these two results agree well with each other. It is clear that the antenna could be operated well at two bands. Input impedance character of the antenna is suitable for the application of two bands.

4.2. Radiation Performances. In Figure 5(a), the radiation pattern of 2.45 GHz is shown. The gain of the circularly polarized antenna is about 4.5 dBi. The front of the near-field antenna is facing positive z-axis direction. The circularly polarized antenna is located on the opposite side of the near-field antenna, so the expected radiation direction is negative z-axis orientation. Additionally, the 26 MHz axial ratio performances can be obtained in Figure 5(b). In Figure 5(a), the measured shape of the radiation pattern agrees well with the simulation one. It is proved that the antenna has good performances of far field. In the next section, the z-orientation magnetic field is concentrated and uniform around the central region of the antenna. The antenna also has good performances for near-field applications.

4.3. Near-Field Performances. The current distribution is shifted between different phases in Figure 6. In contrast to the conventional travelling wave antenna, the current on the loop follows a standing-wave distribution. Magnetic field in the central region will be weak if the current distribution is out of phase. In Figure 6, the current is in phase because of the small electrical length. For the phases of 45°, 90°, and 135°, the current is very strong such that the z-orientation magnetic field is strong synchronously. This conclusion is verified by the comparison between Figures 6 and 7.

Figure 7 shows that the magnetic field is even and centralized in the central region of the antenna for different phases (0°, 45°, 90°, and 135°). Moreover, as a result of the folded terminal, the average current is enhanced on the outer loop and strong magnetic field intensity is obtained. Figure 8 shows the magnetic field distribution for different z. Figure 8 focuses on the magnetic field intensity attenuation along the scale of the z-axis.

Compared with other antennas, it is found that the z-orientation magnetic field of the new antenna is much

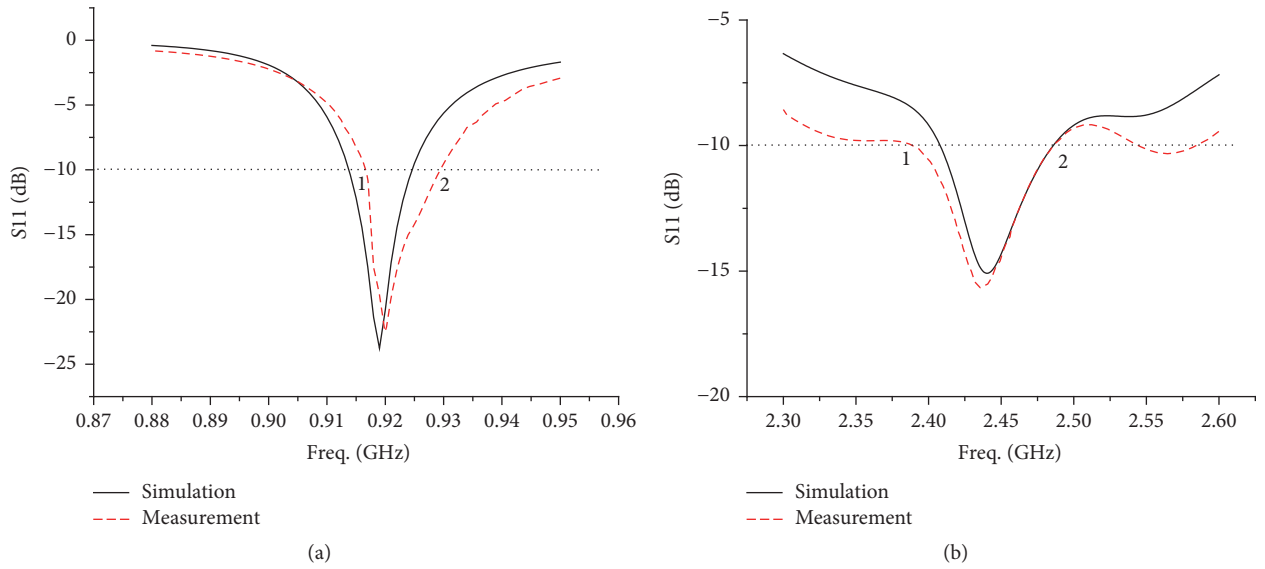

Figure 4: The S11 performances of the antenna at UHF and S band. −10 dB bandwidth of measurement results is marked in two pictures: (a) UHF band, marker 1 = 914 MHz, marker 2 = 932 MHz; (b) 2.45 GHz, marker 1 = 2.37 GHz, marker 2 = 2.48 GHz.

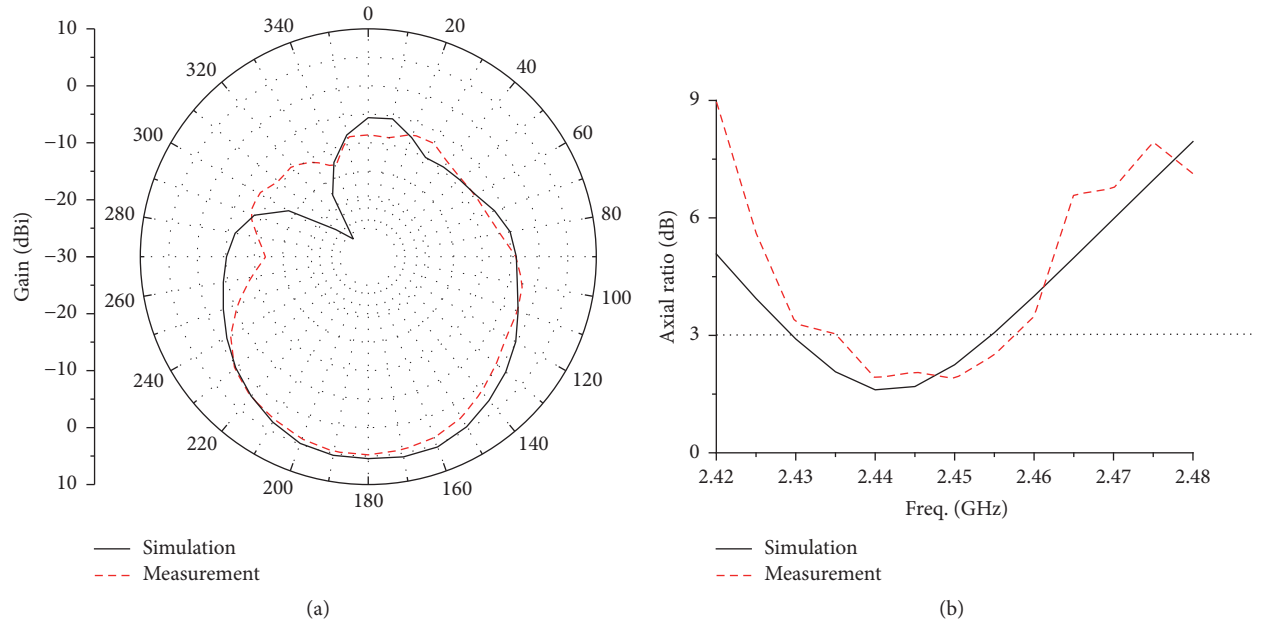

Figure 5: Radiation performances of the antenna at 2.45 GHz: (a) gain pattern and (b) axial ratio of the antenna.

stronger. For example, referring to Figure 8, the central region magnetic field of the new antenna is significantly stronger than that of the proposed antenna in [10] for the same z. At $z = 1$ cm, our antenna generates a magnetic field intensity of 5.2 dBA/m, whereas the antenna in [11] generates only −5 dBA/m. Taking Figure 7 as a reference, the magnetic field in the central region of the antenna is also stronger than that of another broadband antenna proposed in [12]. This shows that the magnetic field intensity of the antenna in [12] is lower than −10 dBA/m at $z = 0.5$ mm, whereas that of our antenna is greater than 0 dBA/m even at $z = 1$ cm. Actually, the magnetic field of the proposed antenna is stronger than most of the UHF near-field antennas [7–13].

4.4. Reading Range Performance. To further verify the near-field performance of the novel antenna, the prototype is used as the reader antenna in a UHF near-field RFID system to detect UHF near-field tags. The measurement system is shown in Figure 9. The proposed antenna is connected to the reader operating at FCC band with 30 dBm output to detect the tag. In Figure 9, the tag is positioned on an 80 mm ∗ 80 mm foam board marked by 1 cm × 1 cm grids.

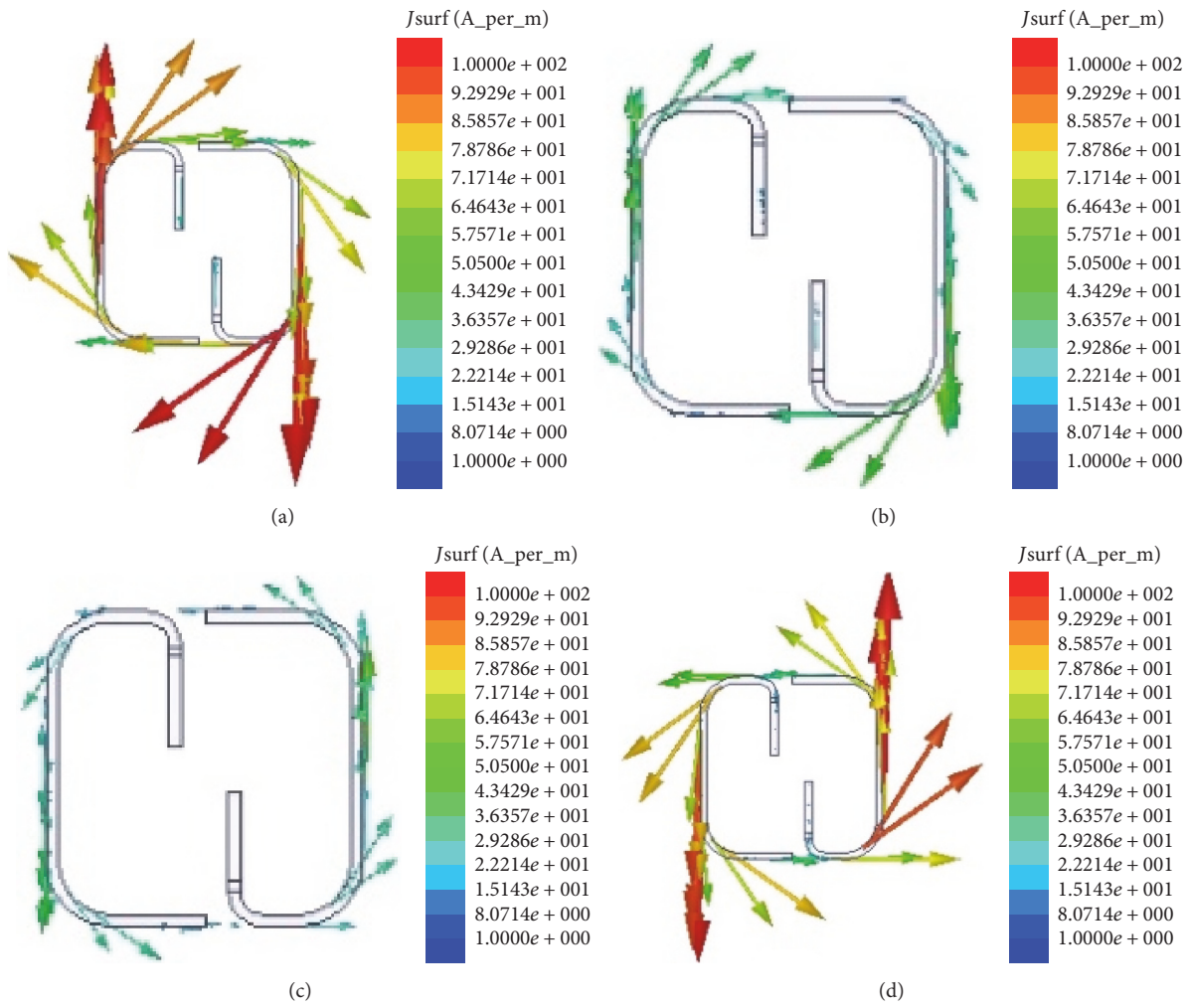

Figure 6: Current distribution on a metal strip at different phases: (a) 0 degrees, (b) 45 degrees, (c) 90 degrees, and (d) 135 degrees.

The data of the correctly detected tag on each intersection of grids were recorded when the top surface of a foam board was fixed at different z.

This paper adopts one annular Impinj J41 tag, which could be activated when the magnetic field intensity of the command signal is stronger than −13 dBA/m. But the tag will be easier activated and quicker read if the magnetic intensity is stronger.

The measurement results for the reading range are presented in Figure 10. By comparison between Figures 10 and 7, it could be seen that, at each z, the reading ranges have an approximate agreement with the magnetic field distribution. The reading distance of the antenna is much longer than most of the RFID near-field antennas.

5. Conclusion

Because of different operation modes and frequencies, it is a challenge to design a UHF near-field RFID antenna with far-field circularly polarized radiation at 2.45 GHz. The applications of the antenna with two operation modes are useful for reduction of the multifunctioned RFID system. The new proposed antenna has demonstrated the capability of producing a strong magnetic field in the near-field region of the antenna with good circularly polarized far-field performances at 2.45 GHz, which is very promising for 920 MHz near-field and 2.45 GHz far-field RFID systems.

Thus, the investigation also has shown that the two operation modes all bring about a strong effect on the input impedance of the antenna. Mutual effects of the near-field and far-field antennas play an important role in the performance of efficiency due to the isolation between the two modes.

Conflicts of Interest

The authors declare that they have no conflicts of interest.

Acknowledgments

This work was supported in part by the National Natural Science Foundation of China (no. 61601373), Natural Science

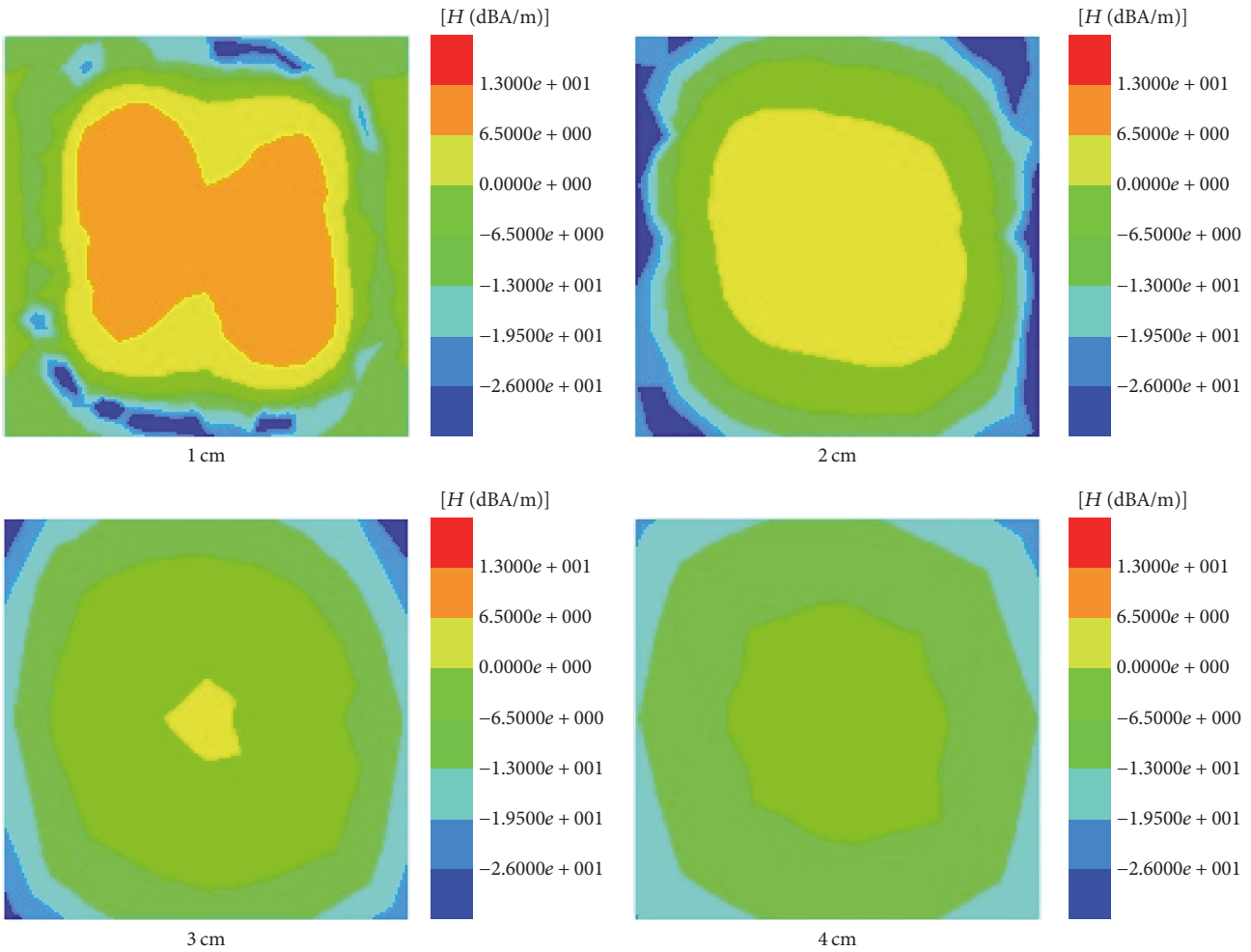

Figure 7: Simulated z-orientation magnetic field distribution at different z. The edge length of the reference plane is also 80 mm.

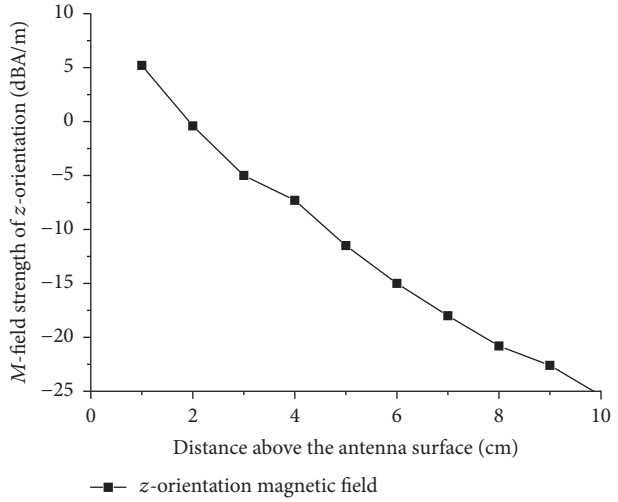

Figure 8: Simulated magnetic field intensity of the antennas along the z-axis.

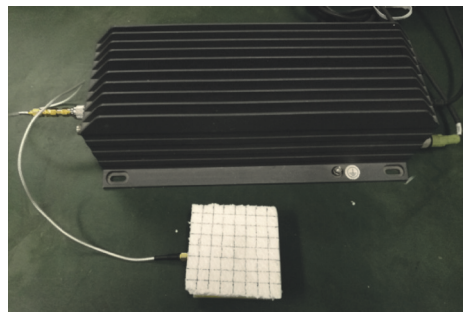

Figure 9: Configuration of the measurement scenario: reader antenna and reader which are connected with a computer.

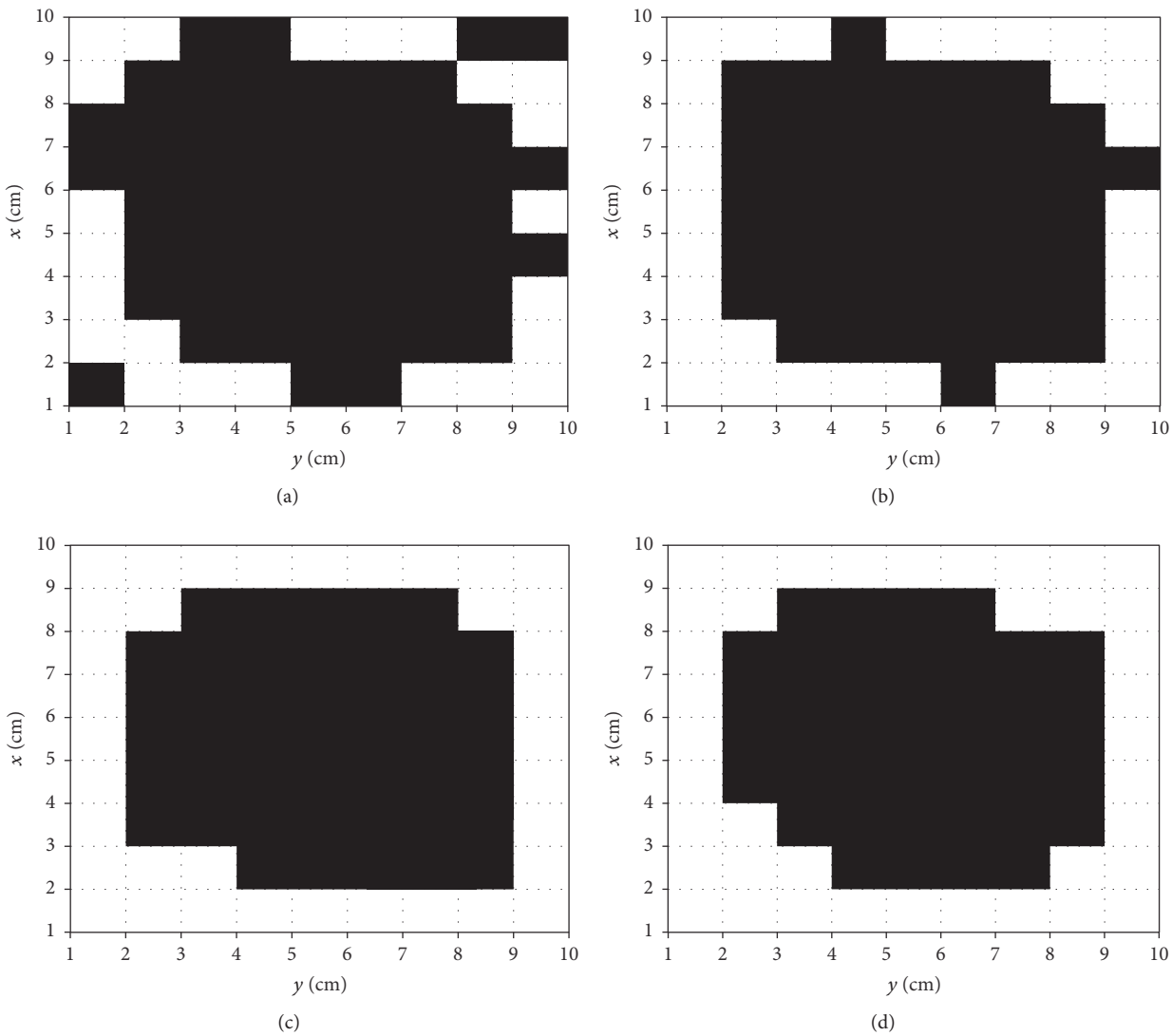

Figure 10: Reading scope of the antenna at different distances, which are 1 cm, 2 cm, 3 cm, and 4 cm. The black grid marks the intersection which could be read when a tag is put on it, and the white grid marks the opposite.

Basic Research Plan of Shaanxi Province (no. 2017JQ6072), and the Aerospace Science and Technology Innovation Fund of China (no. 2016KC080013).

References

[1] R. Want, "An introduction to RFID technology," *IEEE Pervasive Computing*, vol. 5, no. 1, pp. 25–33, 2006.

[2] J. Landt, "The history of RFID," *IEEE Potentials*, vol. 24, no. 4, pp. 8–11, 2005.

[3] X. Li and L. Cao, "Microstrip-based segmented coupling reader antenna for near-field UHF RFID applications," *Microwave and Optical Technology Letters*, vol. 53, no. 8, pp. 1774–1777, 2011.

[4] A. Sharma, I. J. G. Zuazola, J. C. Batchelor, and A. Perallos, "Dual purpose near-and far-field UHF RFID coil antenna with non-uniformly distributed-turns," *IEEE Antennas and Wireless Propagation Letters*, vol. 14, pp. 1342–1345, 2015.

[5] A. L. Borja, A. Belenguer, J. Cascon, and J. R. Kelly, "A reconfigurable passive UHF reader loop antenna for near-field and far-field RFID applications," *IEEE Antennas and Wireless Propagation Letters*, vol. 11, pp. 580–583, 2012.

[6] H.-Y. A. Yim, C.-P. Kong, and K.-K. M. Cheng, "Compact circularly polarised microstrip antenna design for dual-band applications," *Electronics Letters*, vol. 42, no. 7, pp. 380-381, 2006.

[7] Z. Xing, L. Wang, C. Wu, and K. Wei, "Study of broadband near-field antenna for ultra-high frequency radio frequency identification applications," *IET Microwaves, Antennas & Propagation*, vol. 5, no. 14, pp. 1661–1669, 2011.

[8] Z. Xing, K. Wei, L. Wang, and J. Li, "Dual-band RFID antenna for near field of 0.93 GHz and far field of 2.45 GHz," in *Proceedings of the IEEE 5th Asia-Pacific Conference on Antennas and Propagation (APCAP)*, pp. 453-454, Kaohsiung, Taiwan, July 2016.

[9] S. Wang, X. Guan, D. Wang, X. Ma, and Y. Su, "Fast calculation of wide-band responses of complex radar targets," *Progress In Electromagnetics Research*, vol. 68, pp. 185–196, 2007.

[10] L. Shen, W. Zhuang, W. Tang, and J. Ma, "Achieving uniform perpendicular magnetic field distribution for near-field ultra-high frequency radio-frequency identification," *IET Microwaves, Antennas and Propagation*, vol. 10, no. 2, pp. 215–222, 2016.

[11] X.-D. Wei, H.-L. Zhang, and B.-J. Hu, "Novel broadband center-fed UHF near-field RFID reader antenna," *IEEE Antennas and Wireless Propagation Letters*, vol. 14, pp. 703–706, 2015.

[12] Mini Guardrail Antenna Datasheet, https://support.impinj.com/hc/en-us/articles/202755678-Mini-Guardrail-Antenna-Datasheet.

[13] X. Qing, C. K. Goh, and Z. N. Chen, "A broadband UHF near field RFID antenna," *IEEE Transactions on Antennas and Propagation*, vol. 58, no. 24, pp. 3829–3838, 2010.

[14] J. M. J. W. Jayasinghe and D. Uduwawala, "A novel multiband miniature planar inverted F antenna design for bluetooth and WLAN applications," *International Journal of Antennas and Propagation*, vol. 2015, Article ID 970152, 6 pages, 2015.

[15] W. Cai and L. L. Gouveia, "Modeling and simulation of maximum power point tracker in ptolemy," *Journal of Clean Energy Technologies*, pp. 6–9, 2013.

[16] W. Cai, X. Zhou, and X. Cui, "Optimization of a GPU implementation of multi-dimensional RF pulse design algorithm," in *Proceedings of the International Conference on Bioinformatics & Biomedical Engineering*, May, 2011.

[17] W. Cai and F. Shi, "2.4 GHz heterodyne receiver for healthcare application," *International Journal of Pharmacy and Pharmaceutical Sciences*, vol. 8, no. 6, pp. 162–165, 2016.

[18] W. Cai, J. Chan, and D. Garmire, "3-axes MEMS hall-effect sensor," in *Proceedings of the 6th IEEE Sensors Applications Symposium, SAS 2011*, pp. 141–144, February 2011.

[19] C. Phongcharoenpanich and B. Sricharoen, "Dual-band circularly polarized rectangular loop slot antenna for UHF-RFID reader," in *Proceedings of the IEEE International Conference on Wireless Information Technology and Systems, ICWITS 2012*, November 2012.

[20] M. T. Zhang, Y. B. Chen, Y. C. Jiao, and F. S. Zhang, "Dual circularly polarized antenna of compact structure for rfid application," *Journal of Electromagnetic Waves and Applications*, vol. 20, no. 14, pp. 1895–1902, 2006.

[21] Q. Liu, J. Shen, H. Liu, and Y. Liu, "Dual-band circularly-polarized unidirectional patch antenna for RFID reader applications," *Institute of Electrical and Electronics Engineers. Transactions on Antennas and Propagation*, vol. 62, no. 12, pp. 6428–6434, 2014.

[22] C. K. Goh, X. Qing, and Z. N. Chen, "A slotted circularly-polarized patch antenna for near-field and far-field UHF RFID applications," in *Proceedings of the IEEE Antennas and Propagation Society International Symposium, APSURSI 2014*, pp. 1514-1515, July 2014.

[23] J. Anguera, C. Puente, and C. Borja, "Dual frequency broadband microstrip antenna with a reactive loading and stacked elements," *Progress In Electromagnetics Research Letters*, vol. 10, pp. 1–10, 2009.

[24] A. Moleiro, J. Rosa, R. Nunes, and C. Peixeiro, "Dual band microstrip patch antenna element with parasitic for GSM," in *Proceedings of the IEEE Antennas and Propagation Society International Symposium. Transmitting Waves of Progress to the Next Millennium*, pp. 2188–2191, Salt Lake City, UT, USA.